



This discussion paper is/has been under review for the journal Atmospheric Chemistry and Physics (ACP). Please refer to the corresponding final paper in ACP if available.

A global historical ozone data set and signatures of El Niño and the 11-yr solar cycle

S. Brönnimann^{1,2}, J. Bhend³, J. Franke^{1,2}, S. Flückiger², A. M. Fischer⁴,
R. Bleisch⁵, G. Bodeker⁶, B. Hassler^{7,8}, E. Rozanov^{9,10}, and M. Schraner¹¹

¹Oeschger Centre, University of Bern, Bern, Switzerland

²Institute of Geography, University of Bern, Bern, Switzerland

³CSIRO Marine and Atmospheric Research, Aspendale, Australia

⁴Federal Office of Meteorology and Climatology MeteoSwiss, Zurich, Switzerland

⁵Climate and Environmental Physics, Physics Institute, University of Bern, Bern, Switzerland

⁶Bodeker Scientific, Alexandra, Central Otago, New Zealand

⁷Cooperative Institute for Research in Environmental Sciences (CIRES), University of Colorado at Boulder, Boulder, Colorado, USA

⁸NOAA, Earth System Research Laboratory, Chemical Sciences Division, Boulder, Colorado, USA

⁹Physical-Meteorological Observatory Davos/World Radiation Center, Davos, Switzerland

¹⁰Institute for Atmospheric and Climate Science ETH, Zurich, Switzerland

¹¹CSCS, Lugano, Switzerland

A global historical
ozone data set

S. Brönnimann et al.

Title Page

Abstract

Introduction

Conclusions

References

Tables

Figures

◀

▶

◀

▶

Back

Close

Full Screen / Esc

Printer-friendly Version

Interactive Discussion



Received: 21 December 2012 – Accepted: 7 March 2013 – Published: 21 March 2013

Correspondence to: S. Brönnimann (stefan.broennimann@giub.unibe.ch)

Published by Copernicus Publications on behalf of the European Geosciences Union.

ACPD

13, 7767–7809, 2013

**A global historical
ozone data set**

S. Brönnimann et al.

Title Page

Abstract

Introduction

Conclusions

References

Tables

Figures

⏪

⏩

◀

▶

Back

Close

Full Screen / Esc

Printer-friendly Version

Interactive Discussion



Abstract

We present a vertically resolved (with pressure as the vertical coordinate) zonal mean monthly mean global ozone data set spanning the period 1900 to 2008, called HIS-TOZ.1.0. It is based on a new approach that combines information from an ensemble of chemistry climate model (CCM) simulations with historical total ozone information. The CCM simulations incorporate important external drivers of stratospheric chemistry and dynamics (in particular solar and volcanic effects, greenhouse gases and ozone depleting substances, sea-surface temperatures, and the Quasi-Biennial Oscillation). The historical total ozone observations include ground-based measurements from the 1920s onward and satellite observations from 1970 to 1976. An off-line data assimilation approach (Ensemble Square Root Filter) is used to combine model simulations, observations, and information on the observation error. The period starting in 1979 was used for validation with existing ozone data sets and therefore only ground-based measurements were assimilated. Results demonstrate considerable skill from the CCM simulations alone. While the observations provide little additional skill at the full spatio-temporal resolution, they do increase the skill at lower spatio-temporal resolutions and specifically for total ozone. Analyses of HISTOZ.1.0 with respect to the effects of El Niño/Southern Oscillation (ENSO) and of the 11 yr solar cycle on stratospheric ozone from 1934 to 1979 qualitatively confirm previous studies that focussed on the post-1979 period. However, a more pronounced effect of ENSO and slightly weaker effect of the 11 yr solar cycle are found in the earlier period. Several possible future improvements of HISTOZ.1.0 are discussed.

1 Introduction

Stratospheric ozone affects the radiation budget of the atmosphere and therefore needs to be incorporated in climate model simulations. Models usually require a two-dimensional (latitude, pressure) ozone distribution as a boundary condition. As the

ACPD

13, 7767–7809, 2013

A global historical ozone data set

S. Brönnimann et al.

Title Page

Abstract

Introduction

Conclusions

References

Tables

Figures

◀

▶

◀

▶

Back

Close

Full Screen / Esc

Printer-friendly Version

Interactive Discussion



**A global historical
ozone data set**

S. Brönnimann et al.

Title Page

Abstract

Introduction

Conclusions

References

Tables

Figures

◀

▶

◀

▶

Back

Close

Full Screen / Esc

Printer-friendly Version

Interactive Discussion



spatial distribution of ozone changes on different time scales related to external forcings, a transient ozone boundary condition is essential. While in the third Climate Modelling Intercomparison Project (CMIP-3) some models still used a time-invariant ozone climatology (Miller et al., 2006), current model simulations (CMIP5) mostly use a time-dependent ozone data set (Taylor et al., 2012). Since 1979, two- or three-dimensional ozone data sets are available from merging different satellite (or other) observations (e.g. Stolarski and Frith, 2006; Hassler et al., 2009, 2012). For CMIP5 simulations starting in 1850, a global monthly mean two-dimensional ozone data set was produced whose temporal variability was described using a regression approach based on stratospheric chlorine and the 11 yr solar cycle (Cionni et al., 2011). This data set was designed for coupled ocean-atmosphere simulations and consequently does not include interannual variability that arises due to non-forced climate variability. For atmosphere global climate models (AGCMs), or for data analysis, a vertically and meridionally resolved ozone data set would be desirable that is as close to observations as possible and hence also reflects interannual variability, which may arise, e.g. from changes in sea-surface temperatures (SSTs).

Here we present an approach for producing a monthly mean zonal mean vertically resolved global historical ozone data set based on chemistry climate model simulations and historical (ground-based and satellite-based) total column ozone observations using data assimilation techniques. The main aim of this paper is to discuss the approach and point to possible improvements. The product, termed HISTOZ.1.0, is presented and analysed with respect to prominent variability prior to 1979, focusing on El Niño/Southern Oscillation and the 11 yr solar cycle.

The paper is organised as follows. Section 2 describes the approach. Section 3 describes the data used. In Sect. 4 we report on the ancillary processing and analysis steps, starting with an assessment of the model simulations and followed by technical material related to bias corrections. Section 5 focuses on the specification of observation errors, the construction of error covariance matrices, and covariance localisation. In Sect. 6 we present HISTOZ.1.0 and discuss validation results in the post-1979

period. Some prominent variations in the global ozone field such as those due to El Niño/Southern Oscillation (ENSO) and the 11 yr solar cycle are analysed in Sect. 7. Conclusions are drawn in Sect. 8.

2 Method

2.1 Ensemble Square Root Filter

The basis of our approach (sketched schematically in Fig. S1) is an off-line data assimilation procedure as described by Bhend et al. (2012). The approach aims to find an optimal state (in the model space), termed “analysis” or \mathbf{x}_a , starting from a “background” model state \mathbf{x}_b and adding a correction that depends on the observations \mathbf{y} . The observation error covariance \mathbf{R} determines the weight given to each observation. The background error covariance matrix \mathbf{P}^b specifies how deviations in each element of the model state vector are related to deviations in each other element and thus determines how the information from the observations is spread into model space.

We use the Ensemble Square Root Filter (EnSRF, Whitaker and Hamill, 2002), a variant of the Ensemble Kalman Filter (EnKF, e.g. Evensen, 2003), to determine the correction (see Bhend et al., 2012 for the following). In our application, \mathbf{x}_b , a vector of length m , denotes the monthly mean ozone at all grid points (latitudes, levels) for a given time from one simulation (one member) in an initial-condition ensemble simulation. Each member, as well as the ensemble mean, are corrected using the observations \mathbf{y} (all available monthly means for the same time), a vector of length n . In the EnSRF, \mathbf{x}_b is decomposed into the ensemble mean $\overline{\mathbf{x}_b}$ and the deviations therefrom (\mathbf{x}'_b). Similarly, the correction is separated into an ensemble mean correction (Eq. 1) which is identical to the EnKF correction, and a correction of the anomalies from the ensemble mean

Title Page

Abstract

Introduction

Conclusions

References

Tables

Figures

◀

▶

◀

▶

Back

Close

Full Screen / Esc

Printer-friendly Version

Interactive Discussion



(Eq. 2):

$$\bar{\mathbf{x}}_a = \bar{\mathbf{x}}_b + \mathbf{K}(\bar{\mathbf{y}} - \mathbf{H}\bar{\mathbf{x}}_b) \quad (1)$$

$$\mathbf{x}'_a = \mathbf{x}'_b + \tilde{\mathbf{K}}(\mathbf{y}' - \mathbf{H}\mathbf{x}'_b) = (\mathbf{I} - \tilde{\mathbf{K}}\mathbf{H})\mathbf{x}'_b, \text{ with } \mathbf{y}' = 0 \quad (2)$$

5 **H**, a matrix of size $n \times m$, is the Jacobian matrix of the linear observation operator that extracts the observations from the model state \mathbf{x} (see Sect. 2.3). The Kalman gain matrix **K** ($m \times n$) is identical to the gain matrix in the classical EnKF approach (Eq. 3).

$$\mathbf{K} = \mathbf{P}^b \mathbf{H}^T (\mathbf{H} \mathbf{P}^b \mathbf{H}^T + \mathbf{R})^{-1} \quad (3)$$

The gain matrix for the ensemble anomalies is expressed as follows (Eq. 4):

$$10 \tilde{\mathbf{K}} = \mathbf{P}^b \mathbf{H}^T \left[\left(\sqrt{\mathbf{H} \mathbf{P}^b \mathbf{H}^T + \mathbf{R}} \right)^{-1} \right]^T \times \left(\sqrt{\mathbf{H} \mathbf{P}^b \mathbf{H}^T + \mathbf{R} + \sqrt{\mathbf{R}}} \right)^{-1} \quad (4)$$

P^b is the $m \times m$ background error covariance matrix (Sect. 5.3), **R** is the $n \times n$ observation error covariance matrix (Sect. 5.1). We assume that the observation errors are uncorrelated (**R** is diagonal), which allows a serial incorporation of each observation (i.e. **R** becomes a scalar).

15 Note that the analyses are not used as new initial states for the model. Rather, we use existing simulations in an “off-line” approach. Although we lose some of the advantages of data assimilation with this approach, we gain simplicity. The approach can be used a posteriori, i.e. the procedure can be optimised and observations or error information can be updated without the need to repeat the simulations. Since the filter will
20 only be applied once every six months (albeit the resolution of the product is monthly, see Sect. 2.2), the role of initial conditions is small and that of the boundary conditions becomes more important.

2.2 State vector

In most data assimilation approaches, the vector \mathbf{x} describes the model state at a given time. In this study the product is generated at monthly resolution. However, as ozone at middle to high latitudes has strong month-to-month correlation during the summer months of the respective hemisphere (Fioletov and Shepherd, 2003), observations in a given month were allowed to affect neighbouring months in the same season by combining six consecutive months into one state vector \mathbf{x} . In other words, \mathbf{x} contains the monthly and zonally averaged ozone number densities from all grid cells for six months. Sudden steps due to gaps in individual observation records are expected to be smoothed and the sparse information is exploited more fully. Based on the correlation tables in Fioletov and Shepherd (2003), the 6 month seasons are defined as May to October and November to April. Correlations between the seasons are low so that this procedure is not expected to introduce large steps at the transitions of the seasons.

The zonal mean ozone fields comprise 36 latitudes and 30 pressure levels (0.01, 0.05, 0.1, 0.3, 0.5, 1, 1.6, 2.5, 4, 6.3, 10, 15.9, 25.1, 39.8, 63.1, 100, 150, 200, 250, 350, 450, 550, 650, 750, 800, 850, 900, 950, 980, 1000 hPa), of which only 25 levels are used, as ozone is set to zero in the top layer and the four lowermost layers. After combining the data into six month blocks, the final state vector \mathbf{x} has a length of 5400 and the covariance matrix \mathbf{P}^b has around 3×10^7 elements.

2.3 Observation operator

The function $H(\mathbf{x})$ transforms the model space into the observation space:

$$H(\mathbf{x}) = c \cdot \sum_x \max(0, 1 - |\varphi(x) - \varphi(y)|/\Delta\varphi) \cdot \text{mon}(x) \cdot \Delta z(x) \cdot x \quad (5)$$

where $\varphi(x)$ is the latitude of element x of \mathbf{x} , $\Delta\varphi$ is the grid spacing, and $\varphi(y)$ is the latitude of the observation y (i.e. the term $\max(0, 1 - |\varphi(x) - \varphi(y)|/\Delta\varphi)$ provides the weights of a linear interpolation), $\Delta z(x)$ is the layer thickness and the constant $c = 2.6868 \times 10^{16} \text{ molec cm}^{-2}$ converts the result to Dobson Units (DU). The function

Title Page

Abstract

Introduction

Conclusions

References

Tables

Figures

◀

▶

◀

▶

Back

Close

Full Screen / Esc

Printer-friendly Version

Interactive Discussion



$\text{mon}(x)$ selects the month, i.e. mon equals 1 (else 0) if the month of x is the month of the observations. The layer thickness is calculated from geopotential height (GPH) from the ensemble mean. For simplicity (and after finding only a very small dependence on interannual variability), the GPH profile from 1960 was used for all years.

As H expresses a linear combination of the elements of x , the Jacobian matrix of H , termed \mathbf{H} , consists of the coefficients:

$$H(x) = \mathbf{H}x = \hat{y} \quad (6)$$

In our implementation, \mathbf{H} is a vector (because observations are assimilated serially) and its scalar product with x gives the integrated and interpolated ozone column for the latitude and month of the observation.

3 Data sets

3.1 Model simulations

In this study we use an initial condition ensemble of nine simulations from 1900 to 1999 that was performed with the chemistry-climate model SOCOL Version 2 (Schranner et al., 2008). The simulations are described in Fischer et al. (2008b). SOCOL is a combination of the middle atmosphere version of the ECHAM4 spectral AGCM (Manzini and McFarlane, 1998) and the chemistry-transport model MEZON (Egorova et al., 2003). It was run with a spectral truncation of T30 and 39 levels on a hybrid sigma-pressure coordinate system, with the model top at 0.01 hPa. A hybrid numerical advection scheme is used for transporting chemical species (Zubov et al., 1999), with the Prather advection scheme in the vertical (Prather, 1986) and the Semi-Lagrangian scheme in the horizontal direction (Williamson and Rasch, 1989). The model participated in the CCMval validation experiments (SPARC CCMVal, 2010) and the C20C intercomparisons for AGCMs (e.g. Scaife et al., 2008).

Title Page

Abstract

Introduction

Conclusions

References

Tables

Figures

◀

▶

◀

▶

Back

Close

Full Screen / Esc

Printer-friendly Version

Interactive Discussion



**A global historical
ozone data set**

S. Brönnimann et al.

Title Page

Abstract

Introduction

Conclusions

References

Tables

Figures

◀

▶

◀

▶

Back

Close

Full Screen / Esc

Printer-friendly Version

Interactive Discussion



The model was constrained at the boundaries with monthly SSTs and sea ice from the HadISST1 data set (Rayner et al., 2003) and land-surface properties based on Hagemann (2002). Solar variability was prescribed using spectral solar irradiance data from Lean (2000). Greenhouse gases and organic chlorine and bromine containing gases were prescribed in the lowermost five layers. In addition, surface emissions of CO and NO_x were prescribed (see Fischer et al., 2008b for details). Stratospheric aerosols were taken from Sato et al. (1993). The model set-up included a nudging of the Quasi-Biennial Oscillation (QBO) using a preliminary version of the QBO reconstruction by Brönnimann et al. (2007b).

3.2 Ozone observations

3.2.1 Ground-based total column ozone observations

Ground-based measurements of total column ozone have been made since the 1920s (for a review see Brönnimann et al., 2003a). In 1957, the start of the International Geophysical Year (IGY), a global standardized network, employing techniques superior to what had previously been available, was established. Hence we distinguish pre-IGY and post-IGY periods in the following analysis.

For the pre-IGY period, we use all series described by Brönnimann et al. (2003a), comprising several long, homogenised, and semi-continuous series such as those from Arosa since 1926 (Staehelin et al., 1998), Oxford, 1924–1975 (Vogler et al., 2007), Tromsø since the 1930s (Hansen and Svenøe, 2005), Dombås and Oslo from the 1940s (Svendby, 2003), and Spitsbergen, 1950–1963 (Vogler et al., 2006), as well as several shorter series. The latter were re-evaluated as described in Brönnimann et al. (2003b). Those historical data series qualified as “poor” in Brönnimann et al. (2003b) were excluded. In addition, measurements from Gulmarg and Srinagar were excluded due to their poor seasonal coverage. Despite their rather low quality, total column ozone data derived from measurements by the Smithsonian Institution at Table Mountain, California (Brönnimann, 2005) were used because they constitute an

important source of information for the 1920s and 1930s. For the post-IGY period, data were obtained from the World Ozone and Ultraviolet Radiation Data Centre (WOUDC). We chose measurement series with at least 5 complete years prior to 1979 and few instrument changes. In all, total column ozone series at 57 locations were used (see Fig. 1, Table S1). All selected series were also used after 1978 for testing and validation purposes.

Monthly means were calculated as the average of the available observations if at least ten daily values were available. Moreover, at least eight monthly means must be available per sequence (i.e. per series obtained with the same instrument type and observation mode, see Table S1), otherwise the series were discarded. This criterion was necessary to retain enough degrees of freedom for the bias adjustment. Figure 2 gives the number of monthly mean values. The first observations became available in 1925. Until about 1950, measurements from around five sites are available in each month. This number then increases to around ten between 1950 and 1957 and to around 20 to 35 from the IGY onwards.

3.2.2 Backscatter Ultraviolet (BUV) observations

Total column ozone was measured from space starting in 1970 with the Backscatter Ultraviolet (BUV) instrument onboard Nimbus-4 (Heath et al., 1973; Stolarski et al., 1997). Due to battery failure, coverage decreased after the first two years, but data were retrieved until 1976. The data quality is inferior to later missions and the data have only rarely been used in publications. Here we use reprocessed BUV data (Stolarski and Frith, 2006). Comparisons with ground-based total column ozone data were performed to check their quality (see Sect. 5.1). Here, we make use of monthly zonal mean total column ozone in 5° latitude bins. Figure 2 shows the number of available monthly means from BUV. Note that whenever a zonal mean value from BUV was available, no ground-based data from the corresponding 5° latitude belt were assimilated (but all ground-based data were used for the pre-processing steps described in Sect. 4).

Title Page

Abstract

Introduction

Conclusions

References

Tables

Figures

◀

▶

◀

▶

Back

Close

Full Screen / Esc

Printer-friendly Version

Interactive Discussion



3.3 Auxiliary observation-based data

Additional data sets were used in various pre-processing steps. With respect to ozone, we used the monthly BDBP vertically resolved ozone data set (Bodeker et al., 2012), 1979–2007, as a reference. In addition, Version 8 TOMS satellite total column ozone data were used for validation and, in some cases (see Table 1), for calibrating the correction function for the zonal mean adjustment (see Sect. 4.3). Note that no TOMS total column ozone data were assimilated.

For estimating zonal mean total column ozone from a station, we used 200 hPa GPH data from ERA-40 from 1957 to 2002 (Uppala et al., 2005) in a regression framework (see Sect. 4.3). ERA-40 was supplemented back in time by statistically reconstructed upper-level fields from Griesser et al. (2010) which are based on historical upper-air and surface data.

4 Assessment and preparation of model and observation data

4.1 Model assessment

As only total column ozone is assimilated, it is vital that the CCM simulates a realistic vertical distribution of ozone and its covariance structure. We therefore assessed the zonal mean ozone variability in the simulations and specifically the effect of external forcings (for further validation studies see SPARC CCMVal, 2010; Fischer et al., 2008b; Scaife et al., 2008).

A multiple linear regression model was applied to the ensemble mean. As our main focus was to reproduce the effects of dynamical and radiative processes in the northern winter polar stratosphere, the regression model was applied to zonally averaged variables over the winter months, i.e. January to March. The predictor variables, which were computed from the model boundary conditions, comprise two quasi-orthogonal QBO time series (zonal mean equatorial winds at 10 hPa and 30 hPa, the latter with

Title Page

Abstract

Introduction

Conclusions

References

Tables

Figures

◀

▶

◀

▶

Back

Close

Full Screen / Esc

Printer-friendly Version

Interactive Discussion



**A global historical
ozone data set**

S. Brönnimann et al.

Title Page

Abstract

Introduction

Conclusions

References

Tables

Figures

◀

▶

◀

▶

Back

Close

Full Screen / Esc

Printer-friendly Version

Interactive Discussion



a lag of 2 months), total solar irradiance, stratospheric aerosol optical depth in the layer between 15 and 35 km altitude, greenhouse gas concentrations, and equivalent effective stratospheric chlorine. From the SST fields, indices for El Niño (NINO3.4 index with one month lead time), the Pacific Decadal Oscillation (PDO, Mantua et al., 1997), and the Atlantic Multidecadal Oscillation (AMO, Enfield et al., 2001) were computed as additional predictor variables. The regression-based validation was applied to different simulated variables of SOCOL, but for brevity's sake we only discuss the outcome for ozone. The patterns of ozone changes associated with each of the regression model basis functions (predictor variables) are shown in Fig. 3.

The well-documented relation of ozone to the QBO (e.g. Baldwin et al., 2001) with a dipole-structure over the equatorial stratosphere and decreases in ozone over the whole Northern Hemisphere is well captured in SOCOL. This is also the case for the response to solar variability that exhibits strong increases in ozone in the tropical upper stratosphere with an increase in solar activity, in line with Hood and Soukharev (2012). Regarding stratospheric aerosol loading, ozone shows a positive response to increased aerosols over much of the northern hemispheric stratosphere. While this may be surprising at first sight, this behaviour can be understood by the fact that the stratospheric aerosol facilitates heterogeneous activation of halogen containing species while suppressing the reactive nitrogen oxides. Therefore, different catalytic chemical cycles are dominant depending on the stratospheric burden of ozone depleting substances (Tie and Brasseur, 1995). This becomes relevant when studying the full 20th century with a number of large volcanic eruptions in the first decades of the century with no anthropogenic halogens in the stratosphere. In this case ozone increase caused by the deactivation of reactive nitrogen can dominate. As expected, ozone shows a strong anti-correlation with effective stratospheric chlorine, over the whole Northern Hemisphere. Finally, the response to ENSO can be best described by a change in the strength of the Brewer–Dobson circulation (BDC) (e.g. Fischer et al., 2008a; Hood and Soukharev, 2012) that leads to a ozone decrease in the tropical lower stratosphere and strengthened transport of equatorial ozone towards to the North Pole.

These results show that the model captures well the effect of the boundary conditions on ozone. As a result, we expect that some skill over and above that available from the climatology will result from use of the CCM alone, without yet incorporating observations.

5 4.2 Debiasing of model data

Ozone in SOCOL has a seasonally varying bias in its climatology relative to the BDBP validation data set. We removed the bias by means of a regression model that was fitted in the overlapping period 1979–1999 and applied to the preceding period (the bias consists of an ozone-invariant part and one part that is dependent on the modelled ozone amount). The results of this step are shown in Fig. 4 for two levels in three different zonally averaged regions. In general, the debiasing works well and brings the time series closer to the observations. There is, in general, good agreement with respect to the interannual variability (the agreement is solely due to boundary conditions). Yet, in some regions and levels, the trends and/or seasonality do not agree well.

15 4.3 Adjustment of ground-based total ozone to zonal means

The ground based total column ozone data represent ozone at a given location, whereas the assimilation requires zonal averages. Because station data are too sparse to form averages over latitude bands, the data from each station were adjusted to represent the zonal mean total ozone of the corresponding latitude. We assumed that the deviation of total ozone at a given location from its mean seasonal cycle has a large-scale, zonal mean contribution which arises, for instance, from changes in the BDC, and a zonally non-uniform change that results from an ozone redistribution in the lowermost stratosphere. To account for the latter, we assumed that the deviation N^* of total ozone from its zonal mean $[N]$ is related to the deviation Z^* of 200 hPa GPH from its zonal mean $[Z]$. Previous work has shown the strong relation between midlatitude total ozone and 200 hPa GPH (Brönnimann et al., 2000) in all seasons. For each calendar

Title Page

Abstract

Introduction

Conclusions

References

Tables

Figures

◀

▶

◀

▶

Back

Close

Full Screen / Esc

Printer-friendly Version

Interactive Discussion



month, we fitted the regression model:

$$N = c_0 + c_1[Z] + c_2Z^* + \varepsilon, \quad (7)$$

from which $[N]$ can be estimated as $N - c_2Z^*$. To test the approach, the algorithm was applied to TOMS total column ozone and ERA-40 200 hPa GPH data for the period 1979–2000. Figure 5 shows the results for two selected months, February 1999 and August 1980. Although the zonally asymmetric features are weakened (in some cases considerably), part of the zonal asymmetry remains. This remaining structure must be accounted for in the calculation of the observation error (see Sect. 5.1).

4.4 Debiasing of total column ozone data

Recall that the model data were debiased with respect to BDBP in the overlapping period. A similar debiasing is necessary for the total column ozone observations (both ground-based and BUV satellite data). We applied H to the debiased model data \mathbf{x}_b and calculated the difference from observations, i.e. $\mathbf{y} - H(\mathbf{x}_b)$ (BDBP could not be used instead of \mathbf{x}_b as many observation series do not overlap with BDBP). To this difference we fitted in each sequence (i.e. each part of a series that was obtained with the same instrument type and observation mode, see Table 1) the first harmonic of the seasonal cycle using least squares regression and subtracted it from the observations.

All processing steps are summarized, using Rome as an example site, in Fig. 6 (top, note that November–April averages are shown here). The zonal correction (dashed) removes some of the variance of the original series (solid). The debiasing (dotted) does not change the variance but brings the curve closer to $H(\mathbf{x}_b)$ (blue). The middle panel shows debiased observations (solid) as well as $H(\mathbf{x}_b)$ (dashed, November–April averages) for three sites (Rome, Nashville, Tateno) and one BUV series (35°–40° N). All series represent similar latitudes. As a consequence, $H(\mathbf{x}_b)$ is quite similar for all sites. The zonal correction should bring the three observation-based series (which are at very different longitudes) closer together. Indeed, the mutual correlations increase

Title Page

Abstract

Introduction

Conclusions

References

Tables

Figures

◀

▶

◀

▶

Back

Close

Full Screen / Esc

Printer-friendly Version

Interactive Discussion



from 0.6–0.7 to 0.65–0.8, but differences remain. BUV shows an outlier (winter 1975), which is related to an observation error (see Sect. 5.2.).

5 Error covariance matrices

5.1 Observation error covariance

R is a diagonal matrix that contains the observation error variances. We assume that the error variance consists of several sources of errors which can be quantified individually and which are independent from each other:

$$\sigma_{\text{obs_error}}^2 = \sigma_{\text{obs_zenith}}^2 + \sigma_m^2 + \sigma_{\text{zonal}}^2. \quad (8)$$

Here $\sigma_{\text{obs_zenith}}$ is the error of a zenith observation, which is mainly an instrumental error, σ_m is the error that depends on the air mass and hence on the atmosphere, and σ_{zonal} is the error due to insufficient adjustment to zonal means. The error $\sigma_{\text{obs_zenith}}$ is estimated from the corresponding literature (Tab. S1). For instance, the quality statements for “precision” in Brönnimann et al. (2003b) were translated in the following way: 4 DU for “excellent”, 8 DU for “very good”, 12 DU for “good” and 16 DU for “fair” (stations rated as “poor” were not considered at all). The Table Mountain data from the Smithsonian Institution received an error of 20 DU. We proceeded similarly for other series, attributing 4 DU to the homogenized long-term series and 6 DU to all other post-1957 data (see Table 1). This is broadly consistent with the literature (Mérige, 1989; Brönnimann et al., 2003b), although most references do not specifically refer to monthly means.

Comparisons between BUV and ground-based total column ozone data were performed in the late 1970s and early 1980s, but focusing on the accuracy rather than the precision (Mérige, 1989; WMO, 1980, 1983). Differences were found to lie in the range of 17 DU or larger than 3%.

For estimating $\sigma_{\text{obs_zenith}}$ and σ_m for BUV we compared daily ground-based total column ozone data from Arosa and Oxford with BUV total column ozone data distance-

Title Page

Abstract

Introduction

Conclusions

References

Tables

Figures

◀

▶

◀

▶

Back

Close

Full Screen / Esc

Printer-friendly Version

Interactive Discussion



A global historical
ozone data set

S. Brönnimann et al.

Title Page

Abstract

Introduction

Conclusions

References

Tables

Figures

◀

▶

◀

▶

Back

Close

Full Screen / Esc

Printer-friendly Version

Interactive Discussion



weighted within a $4^\circ \times 4^\circ$ square around these stations from the same day (R. Bleisch, unpublished report). A regression approach was performed incorporating a linear trend as well as dependencies on total ozone, air mass, and reflectivity (from BUV data) or cloud cover (estimated from ground based stations). Results showed that by far the most important contributor to the variations in differences is air mass. Smaller influences were found for the trend and (in the case of Oxford) for total column ozone. The standard deviation of the (daily) residuals was between 10 and 15 DU. Based on these results we set $\sigma_{\text{obs.zenith}}$ for monthly means to 10 DU for BUV data. Given our confidence in the Arosa series (Staehelin et al., 1998), we attribute most of the air mass dependent error to the BUV data and assume a 2 % error per unit air mass for BUV and a 0.5 % error for ground-based data (assuming local noon for all observations).

For determining σ_{zonal} we analysed the zonal standard deviation of the adjusted TOMS data (see Sect. 4.3). Smoothing the dependence on latitude and on the seasonal cycle resulted in an estimation of σ_{zonal} (Fig. S2). Note that to this point errors were considered to be uncorrelated. This is, however, not the case for σ_{zonal} , which is similar for two stations close to each other. Rather than letting **R** become non-diagonal, we accounted for this problem by multiplying σ_{zonal} for each station with a weight that depends on the distances D_i to all stations i , including the station itself. These distances were first transformed using an exponential function (see Eq. 9) with a length scale L of 1000 km (representing a typical decorrelation scale for upper-level variables, Griesser et al., 2010) and then summed over all stations in all latitude bands. Hence, **R** is then a diagonal matrix with r for each observation in the diagonal:

$$r = \sigma_{\text{obs.zenith}}^2 + \sigma_{\text{m}}^2 + \sigma_{\text{zonal}}^2 \sum_i \exp\left(\frac{-D_i^2}{2L^2}\right) \quad (9)$$

5.2 Assessment of errors

The consistency of errors was assessed monthly by analysing the fraction of differences $|\mathbf{y} - \mathbf{H}\mathbf{x}_{\text{b}}|$ larger than $2\sqrt{(\sigma_{\text{obs.error}}^2 + \sigma_{\text{ensemble}}^2)}$ for the series in Fig. 6 (Rome,

[Title Page](#)[Abstract](#)[Introduction](#)[Conclusions](#)[References](#)[Tables](#)[Figures](#)[◀](#)[▶](#)[◀](#)[▶](#)[Back](#)[Close](#)[Full Screen / Esc](#)[Printer-friendly Version](#)[Interactive Discussion](#)

Nashville, Tateno, and corresponding BUV data). Assuming a Gaussian distribution of errors and no bias, a fraction of 5% is expected. We find fractions of 7%, 5%, 19%, and 8%, respectively. The high fraction for Tateno could be due to a remaining seasonally varying bias. The assimilation procedure requires that $|\mathbf{y} - H(\mathbf{x}_b)| <$

5 $3\sqrt{(\sigma_{\text{obs_error}}^2 + \sigma_{\text{ensemble}}^2)}$. As a consequence, the erroneous BUV data are not assimilated and the fractions are further reduced. Hence, our error estimates that are based on metadata and independent analyses are broadly consistent with the differences, but further improvements on the side of the observations (debiasing, homogenisation, outlier screening) might be beneficial.

10 5.3 Background error covariance

The background covariance matrix \mathbf{P}^b was estimated from the ensemble covariance matrix. Unfortunately, our ensemble is small (nine members). Spurious correlations may occur far off the diagonal which may affect the results. A localisation of the matrix (or similar adjustment) is therefore necessary. The covariance matrix was localised in

15 latitude and time, leaving the altitude dimension unaltered. The localisation followed the principle of distance weighting as above (see also Bhend et al., 2012). Ozone is strongly affected by the BDC, which shows a distinct, seasonally dependent, latitudinal structure. Therefore the distance weighting was altered to allow long-range correlations during times and regions when the BDC is active. We accounted for this by weighting

20 the distance with a function a in the following way:

$$w_{i,j} = \sqrt{a_i a_j} \exp\left(\frac{-D^2}{2L_1^2}\right) + \sqrt{(1-a_i)(1-a_j)} \exp\left(\frac{-D^2}{2L_2^2}\right) \quad (10)$$

Here, $w_{i,j}$ represent scaling factors applied to the covariances between elements i and j of \mathbf{x}_b . D in this case is the latitudinal distance (in degrees; L_1 is set to 20° , L_2 is set to 40°). The function a depends on the season, switching the sign of the latitude axis

25 between boreal winter (November–April) and austral winter (May–October). Function a

and the resulting matrix of scaling factors are shown in Fig. S2. Localisation was also applied in time, setting L to 3 months (consistent with Fioletov and Shepherd, 2003).

6 Results

6.1 The HISTOZ.1.0 data

5 The assimilation corrects the zonally averaged background ozone field in such a way as to best match all adjusted total column ozone observations. Corrections are usually largest at the locations of observations and at altitudes of high ozone variability. However, large corrections sometimes also occur in polar regions, even though little information is available (see Fig. S3 for four example months). In addition, corrections of
10 opposite sign are sometimes found equatorward of the assimilated information, pointing to the important role of \mathbf{P}^b .

Figure 6 (bottom) shows results for the zonally adjusted, debiased total column ozone average from Rome, Nashville, Tateno and the corresponding series from \mathbf{x}_a and \mathbf{x}_b (and $\overline{\mathbf{x}}_a$ and $\overline{\mathbf{x}}_b$). It is apparent that \mathbf{x}_a is much closer to the observations than
15 \mathbf{x}_b . The same holds for $\overline{\mathbf{x}}_a$ and $\overline{\mathbf{x}}_b$. Correlations with observations increase from 0.69 to 0.90. The ensemble spread also decreases considerably. The observations very often lie outside the ensemble spread and hence the model might be overconfident. However, the observation error is not accounted for in this figure (assuming uncorrelated errors, the latter is around 2.5 DU). No sudden jumps in the corrections are found
20 during the time of season transition.

The HISTOZ.1.0 ensemble mean at 25.1 hPa is compared to the data sets by Cionni et al. (2011) (interpolated to 25.1 hPa) and BDBP (from 1979 onward) (Fig. 7) in the form of a latitude time cross-sections. As expected, HISTOZ.1.0 shows clear interannual variability which is lacking in the Cionni et al. (2011) data by construction. The interannual variability in HISTOZ.1.0 is already seen in the first subperiod plotted (1901–
25 1926, i.e. before observations are assimilated), generated by the model boundary con-

Title Page

Abstract

Introduction

Conclusions

References

Tables

Figures

◀

▶

◀

▶

Back

Close

Full Screen / Esc

Printer-friendly Version

Interactive Discussion



ditions. In the last period, i.e. from 1979 onward the agreement between HISTOZ.1.0 and BDBP is very good for the tropical and subtropical regions, but differences are found over the polar regions, especially Antarctica, where HISTOZ.1.0 shows lower minimum values than BDBP.

6.2 Validation using quasi-independent data

In the following, the agreement between HISTOZ.1.0 and quasi-independent data sets is assessed more quantitatively. We use the reduction of error RE (see Cook et al., 1994) as a measure of skill. RE measures the squared differences between the candidate data set and “truth” (a validation data set) and compares this statistic with a “no knowledge prediction” h_0 . For h_0 , RE is 0, positive values thus indicate improvement over the no knowledge prediction. In our application, we use the debiased model background (\bar{x}_b is used for evaluating \bar{x}_a , x_b for x_a) as well as its 1979–1999 climatology as h_0 . The former indicates the skill added by the assimilation while the latter indicates the total skill (model plus assimilation). Note that x_b is rather smooth and that RE tends to punish the addition of variance.

As “truth” we use TOMS for total column ozone and BDBP for the vertical ozone distribution. The analysis was performed for the period 1979–1999. During this period, total column ozone observations from around 30 stations were assimilated, which is typical for the post-1957 period. Note that the validation period contains two volcanic eruptions, anthropogenically driven ozone depletion, and strong trends in atmospheric circulation (e.g. positive trends in the North Atlantic Oscillation) that are generally not well depicted by climate models (e.g. Scaife et al., 2008).

The validation against TOMS zonal mean total column ozone shows mostly positive RE values (Fig. 8), indicating that that HISTOZ.1.0 is mostly closer to TOMS than \bar{x}_b . With respect to the 1979–1999 climatology of x_b , RE reaches values between 0.3 and 0.6, indicating the total skill of the product. The high skill in the equatorial zone is arguably due to the well-modelled effect of the QBO on ozone. Using x_b as h_0 , values are close to 0 in the tropics (where almost no station data are assimilated) and around

Title Page

Abstract

Introduction

Conclusions

References

Tables

Figures

◀

▶

◀

▶

Back

Close

Full Screen / Esc

Printer-friendly Version

Interactive Discussion



0.2–0.5 in the extratropics. This skill results entirely from assimilating observations. The skill for the ensemble mean is mostly higher than the skill for the individual ensemble members, but the latitudinal structure is very similar.

The validation of the vertical structure using BDBP as “truth” (here we only analyse the ensemble mean) shows much lower RE values (Fig. 9). There is skill relative to climatology, but mostly only on a seasonal mean basis. This suggests that most of the skill comes from the CCM simulations, which show stronger responses to boundary conditions on seasonal-to-interannual than on month-to-month time scales. Relative to \bar{x}_b there is hardly any skill. Although the assimilation correctly increases or decreases the amount of ozone in the column for a given latitude, it may put the difference at a wrong altitude, thus decreasing RE. The fact that the covariance matrix was not localised in the vertical dimension may contribute to this result. Degrading the spatio-temporal resolution (seasonal mean, 10° latitude bins, 5 altitude levels) before calculating RE leads to higher skill (Fig. 9).

In all, the results show that HISTOZ.1.0 has considerable skill for total column ozone or for the seasonally averaged vertical distribution on a coarse grid. There is however no skill at the full vertical resolution on a month-to-month scale. As only total column ozone is assimilated, skill in the vertical structure (with respect to x_b) can only come through the background error covariance matrix P^b , pointing to the need to further improve the specification of this matrix. Another reason for low skill is that x_b (used as h_0) was debiased with respect to the BDBP using the same time period as for the validation (unlike the debiasing for y) with the result that its error is small by construction. The skill added by the observations is largest in the lower stratosphere of the midlatitudes where dynamically induced ozone changes are large and observations are available.

7 Analyses

In this section two analyses of HISTOZ.1.0 are presented. They concern the effects of the El Niño/Southern Oscillation (Sect. 7.1) and of the 11-yr solar cycle (Sect. 7.2.) on

Title Page

Abstract

Introduction

Conclusions

References

Tables

Figures

◀

▶

◀

▶

Back

Close

Full Screen / Esc

Printer-friendly Version

Interactive Discussion



ozone. There is ample literature for both effects, but based primarily on the last 30 yr, which unfortunately also carry other strong external signals (volcanic eruptions, ozone depletion, greenhouse gases). HISTOZ.1.0 provides an opportunity to analyse these effects in an independent period that is less disturbed by other forcings, but it does not allow separating the contributions of model and observations to the results.

7.1 El Niño/Southern Oscillation (ENSO)

It has been suggested that ENSO affects the distribution of ozone in the stratosphere by changing the strength of the BDC (Sassi et al., 2004; Manzini et al., 2004; Brönnimann et al., 2004). The SOCOL model (Fischer et al., 2008a), as well as the simulations used here (Fischer et al., 2008b), have been assessed for the effects of ENSO on ozone (see also Fig. 3). Here we focus on one particular, very strong event, namely the ENSO cycle 1939–1944 with the strong and long-lasting El Niño event in 1940–1942 (Brönnimann et al., 2004). We contrast the mean ozone values for El Niño event 1940–1942 with the averages of the years 1939, 1943 and 1944, during which La Niña was present. The model simulations correctly simulate an increase in ozone in the extratropics in boreal winter and a decrease in the tropics, but the differences vanish when analysing calendar year averages (Fig. 10, upper left). In contrast, the observations show an increase in the annual means (Brönnimann et al., 2004).

In HISTOZ.1.0, after assimilating the observations (Fig. 10b), the ENSO signature is more pronounced. The difference is shown in Fig. 10c, again indicating the locations of stations whose data were assimilated. As expected, ozone is elevated at latitudes where observations are available. Interestingly, an even more pronounced signal is found for the polar regions. Furthermore, ozone decreases in the tropics, although no observations are available from that region. This is consistent with a strengthening of the BDC, showing that the correction resulting from the assimilation is physically meaningful.

Most previous studies on the ozone response to ENSO have focused on the period after 1979. However, two of the El Niño events during this period where concurrent

Title Page

Abstract

Introduction

Conclusions

References

Tables

Figures

◀

▶

◀

▶

Back

Close

Full Screen / Esc

Printer-friendly Version

Interactive Discussion



A global historical ozone data set

S. Brönnimann et al.

Title Page

Abstract

Introduction

Conclusions

References

Tables

Figures

◀

▶

◀

▶

Back

Close

Full Screen / Esc

Printer-friendly Version

Interactive Discussion



with volcanic eruptions, which may obscure a clean attribution to ENSO, and not many other strong events have been observed. Using HISTOZ.1.0 we analysed the average ozone fields in January–March and composited all strong El Niño winters after 1934 (to ensure a minimum number of assimilated observations) minus strong La Niña winters using the list given in Brönnimann et al. (2007a) (see Table 1). The difference (Fig. 10d) shows a very prominent ozone signature with an increase in the northern extratropics and a decrease in the tropics (relative deviations are shown in Fig. S4). This pattern, reflecting an increase in strength of the BDC, is consistent with the literature (see Sassi et al., 2004; Manzini et al., 2004; Brönnimann et al., 2004; Fischer et al., 2008b). The composite of three El Niño and three La Niña events after 1979 from BDBP (Fig. 10e) shows a signal that is much less clear and even shows a decrease in northern high latitudes.

7.2 The 11-yr sunspot cycle

Analyses have also been performed with respect to the effect of the 11 yr solar cycle. Rather than reconstructed total solar irradiance from Lean (2000), which is only annually resolved, we used the monthly International Sunspot Number record, available from the Royal Observatory of Belgium's website (<http://sidc.oma.be/sunspot-data/SIDCpub.php>) as the proxy for solar activity. After smoothing the series with a 24 month moving average, we chose periods of 24 consecutive months of maximum and minimum activity in the 11 yr sunspot cycle (Table 2), subdivided into pre-1979 (4 cycles, analysed in HISTOZ.1.0) and post-1979 periods (3 cycles, BDBP). Note that using Lean (2000) total solar irradiance, the same maxima and minima would be found within the uncertainty of the temporal resolution.

The post-1979 period shows an ozone increase throughout the stratosphere with increasing solar activity, strongest in the lower stratosphere (in number density) or upper stratosphere (in mixing ratio, see also Fig. 3). The average difference in x_b in the pre-1979 period (Fig. 11) shows a similar pattern, although the increase in the Northern Hemisphere is no longer uniform. Compared to x_b , the signature in HISTOZ.1.0 is

slightly weaker (relative deviations are shown in Fig. S4). In all, the new results confirm the findings from previous studies based on the post-1979 period. Note that the role of the background fields and the observations cannot be distinguished in this approach.

8 Conclusions and outlook

In this paper we have produced, validated, and analysed a two-dimensional ozone data set from 1900–2008 termed HISTOZ.1.0 that can be used as a boundary condition for climate model simulations. The data set is based on chemistry-climate model simulations up to 1925 and an off-line Ensemble Kalman Filter approach, combining the simulations with historical total column ozone data afterwards. Independent validation suggests that the data set has high skill relative to a climatology. Relative to the model background, additional skill is only found for total column ozone or for the seasonal mean ozone distribution on a coarse resolution, while no additional skill is found at the full temporal and spatial resolution.

HISTOZ.1.0 supports analyses of the effects of ENSO and the 11 yr solar cycle on ozone in periods that have not yet been previously studied. Importantly, the 1930s to 1970s period studied here, unlike the satellite period that is studied in most other publications, is much less strongly affected by volcanic eruptions, ozone depletion, and greenhouse gas emissions. Our results largely confirm previous studies. In the case of ENSO, the signature is more robust. A clear strengthening of the BDC during El Niño winters relative to La Niña winters is found. High solar irradiance elevates ozone throughout the stratosphere, again consistent with previous studies.

Several shortcomings were identified and improvements could be explored for future versions of the data set, comprising the number of ensemble members, and the quality of the simulations themselves, as well as details in the set-up of the assimilation such as the debiasing of observations, the localisation of the background error covariance matrix, or the incorporation of a non-diagonal \mathbf{R} matrix. Using the same general approach (outlined by Bhend et al., 2012), it might also be possible to assimilate

Title Page

Abstract

Introduction

Conclusions

References

Tables

Figures

◀

▶

◀

▶

Back

Close

Full Screen / Esc

Printer-friendly Version

Interactive Discussion



late upper-air information to better constrain ozone or to generate 3-dimensional ozone distributions.

Supplementary material related to this article is available online at:

<http://www.atmos-chem-phys-discuss.net/13/7767/2013/>

[acpd-13-7767-2013-supplement.pdf](#)

Acknowledgements. This work was supported by the Swiss National Science Foundation (Siner-
ergia project FUPSOL and through the NCCR Climate PALVAREX III project) and EU-FP7
project ERACLIM. We would like to acknowledge WOUDC and NASA for providing ozone
data, ECMWF for the ERA-40 data. HISTOZ.1.0 can be downloaded from [ftp://ftp.unibe.ch/
giub/Broennimann/HISTOZ/](ftp://ftp.unibe.ch/giub/Broennimann/HISTOZ/).

References

Baldwin, M. P., Gray, L. J., Dunkerton, T. J., Hamilton, K., Haynes, P. H., Randel, W. J.,
Holton, J. R., Alexander, M. J., Hirota, I., Horinouchi, T., Jones, D. B. A., Kinnerson, J. S.,
Marquardt, C., Sato K., and Takahashi, M.: The quasi-biennial oscillation, *Rev. Geophys.*, 39,
179–229, 2001.

Bhend, J., Franke, J., Folini, D., Wild, M., and Brönnimann, S.: An ensemble-based approach
to climate reconstructions, *Clim. Past*, 8, 963–976, doi:10.5194/cp-8-963-2012, 2012.

Brönnimann, S.: Interactive comment on “Detection and measurement of total ozone from stel-
lar spectra: Paper 2. Historic data from 1935–1942” by R. E. M. Griffin, *Atmos. Chem. Phys.*
Discuss., 5, S4045–S4048, 2005.

Brönnimann, S., Luterbacher, J., Schmutz, C., Wanner H., and Staehelin, J.: Variability of total
ozone at Arosa, Switzerland, since 1931 related to atmospheric circulation indices, *Geophys.*
Res. Lett., 27, 2213–2216, 2000.

Brönnimann S., Staehelin, J., Farmer, S. F. G., Cain, J. C., Svendby, T. M., and Svenøe, T.: Total
ozone observations prior to the IGY. I: A history, *Q. J. Roy. Meteorol. Soc.*, 129, 2797–2817,
2003a.

ACPD

13, 7767–7809, 2013

**A global historical
ozone data set**

S. Brönnimann et al.

Title Page

Abstract

Introduction

Conclusions

References

Tables

Figures

◀

▶

◀

▶

Back

Close

Full Screen / Esc

Printer-friendly Version

Interactive Discussion



**A global historical
ozone data set**

S. Brönnimann et al.

[Title Page](#)[Abstract](#)[Introduction](#)[Conclusions](#)[References](#)[Tables](#)[Figures](#)[◀](#)[▶](#)[◀](#)[▶](#)[Back](#)[Close](#)[Full Screen / Esc](#)[Printer-friendly Version](#)[Interactive Discussion](#)

- Brönnimann S., Cain, J. C., Staehelin, J., Farmer, S. F. G.: Total ozone observations prior to the IGY. II: Data and quality, *Q. J. Roy. Meteorol. Soc.*, 129, 2819–2843, 2003b.
- Brönnimann, S., Luterbacher, J., Staehelin, J., Svendby, T. M., Hansen G., and Svenøe, T.: Extreme climate of the global troposphere and stratosphere in 1940–42 related to El Niño, *Nature*, 431, 971–974, 2004.
- Brönnimann, S., Xoplaki, E., Casty, C., Pauling, A., and Luterbacher, J.: ENSO influence on Europe during the last centuries, *Clim. Dynam.*, 28, 181–197, 2007a.
- Brönnimann, S., Annis, J. L., Vogler C., and Jones, P. D.: Reconstructing the Quasi-Biennial Oscillation back to the early 1900s, *Geophys. Res. Lett.*, 34, L22805, doi:10.1029/2007GL031354, 2007b.
- Cionni, I., Eyring, V., Lamarque, J. F., Randel, W. J., Stevenson, D. S., Wu, F., Bodeker, G. E., Shepherd, T. G., Shindell, D. T., and Waugh, D. W.: Ozone database in support of CMIP5 simulations: results and corresponding radiative forcing, *Atmos. Chem. Phys.*, 11, 11267–11292, doi:10.5194/acp-11-11267-2011, 2011.
- Cook, E. R., Briffa, K. R., and Jones, P. D.: Spatial regression methods in dendroclimatology – a review and comparison of 2 techniques, *Int. J. Climatol.*, 14, 379–402, 1994.
- Egorova, T., Rozanov, E., Zubov, V. A., and Karol, I. L.: Model for investigating ozone trends (MEZON), *Atmos. Ocean Phys.*, 39, 277–292, 2003.
- Enfield, D. B., Mestas-Nunez, A. M., and Trimble, P. J.: The Atlantic multidecadal oscillation and its relation to rainfall and river flows in the continental US, *Geophys. Res. Lett.*, 28, 2077–2080, 2001.
- Evensen, G.: The Ensemble Kalman filter: theoretical formulation and practical implementation, *Ocean. Dynam.*, 53, 343–367, doi:10.1007/s10236-003-0036-9, 2003.
- Fioletov, V. E. and Shepherd, T. G.: Seasonal persistence of midlatitude total ozone anomalies, *Geophys. Res. Lett.*, 30, 1417, doi:10.1029/2002GL016739, 2003.
- Fischer, A. M., Shindell, D. T., Winter, B., Bourqui, M. S., Faluvegi, G., Brönnimann, S., Schraner, M., and Rozanov, E.: Stratospheric winter climate response to ENSO in three chemistry-climate models, *Geophys. Res. Lett.*, 35, L13819, doi:10.1029/2008GL034289, 2008a.
- Fischer, A. M., Schraner, M., Rozanov, E., Kenzelmann, P., Schnadt Poberaj, C., Brunner, D., Lustenberger, A., Luo, B. P., Bodeker, G. E., Egorova, T., Schmutz, W., Peter, T., and Brönnimann, S.: Interannual-to-decadal variability of the stratosphere during the 20th cen-

A global historical ozone data set

S. Brönnimann et al.

Title Page

Abstract

Introduction

Conclusions

References

Tables

Figures

◀

▶

◀

▶

Back

Close

Full Screen / Esc

Printer-friendly Version

Interactive Discussion



ture: ensemble simulations with a chemistry-climate model, *Atmos. Chem. Phys.*, 8, 7755–7777, doi:10.5194/acp-8-7755-2008, 2008b.

Griesser, T., Brönnimann, S., Grant, A., Ewen, T., Stickler, A., and Comeaux, J.: Reconstruction of global monthly upper-level temperature and geopotential height fields back to 1880, *J. Climate*, 23, 5590–5609, 2010.

Hagemann, S.: An Improved Land Surface Parameter Dataset for Global and Regional Climate Models, MPI Report 336, Max-Planck-Institut für Meteorologie, Hamburg, 2002.

Hansen, G. and Svenøe, T.: Multilinear regression analysis of the 65-yr Tromsø total ozone series, *J. Geophys. Res.*, 110, D10103, doi:10.1029/2004JD005387, 2005.

Hassler, B., Bodeker, G. E., and Dameris, M.: Technical Note: A new global database of trace gases and aerosols from multiple sources of high vertical resolution measurements, *Atmos. Chem. Phys.*, 8, 5403–5421, doi:10.5194/acp-8-5403-2008, 2008.

Heath, D. F., Mateer, C. L., and Krueger, A. J.: The Nimbus-4 BUV atmospheric ozone experiment – two year's operation, *Pure Appl. Geophys.*, 106–108, 1238–1253, 1973.

Hood, L. L. and Soukharev, B. E.: The lower-stratospheric response to 11-yr solar forcing: coupling to the troposphere–ocean response, *J. Atmos. Sci.*, 69, 1841–1864, 2012.

Lean, J.: Evolution of the sun's spectral irradiance since the Maunder Minimum, *Geophys. Res. Lett.*, 27, 2425–2428, 2000.

Mantua, N. J., Hare, S. R., Zhang, Y., Wallace, J. M., and Francis, R. C.: A Pacific interdecadal climate oscillation with impacts on salmon production, *B. Am. Meteorol. Soc.*, 78, 1069–1079, 1997.

Manzini, E. and McFarlane, N.: The effect of varying the source spectrum of a gravity wave parameterization in a middle atmosphere general circulation model, *J. Geophys. Res.*, 103, 31523–31539, 1998.

Manzini, E., Giorgetta, M. A., Esch, M., Kornblueh, L., and Roeckner, E.: The influence of sea surface temperatures on the Northern winter stratosphere: ensemble simulations with the MAECHAM5 model, *J. Climate*, 19, 3863–3881, 2006.

Mégie, G., Chanin, M. L., Ehhalt, D., Fraser, P., Frederick, J. F., Gille, J. C., McCormick, M. P., and Schoeberl, M.: Global trends, in: *Scientific Assessment of Stratospheric Ozone: 1989*, vol. 1, World Meteorological Organization Global Ozone Research and Monitoring Project, Report no. 20, World Meteorological Organization, Geneva, 1989.

A global historical ozone data set

S. Brönnimann et al.

Title Page

Abstract

Introduction

Conclusions

References

Tables

Figures

◀

▶

◀

▶

Back

Close

Full Screen / Esc

Printer-friendly Version

Interactive Discussion



- Miller, R. L., Schmidt, G. A., and Shindell, D. T.: Forced annular variations in the 20th century intergovernmental panel on climate change fourth assessment report models, *J. Geophys. Res.*, 111, D18101, doi:10.1029/2005JD006323, 2006.
- Prather, M. J.: Numerical advection by conservation of 2Nd-order moments, *J. Geophys. Res.*, 91, 6671–6681, 1986.
- Rayner, N. A., Parker, D. E., Horton, E. B., Folland, C. K., Alexander, L. V., Rowell, D. P., Kent, E. C., and Kaplan, A.: Global analyses of sea surface temperature, sea ice, and night marine air temperature since the late nineteenth century, *J. Geophys. Res.*, 108, 4407, doi:10.1029/2002JD002670, 2003.
- Sassi, F., Kinnison, D., Boville, B. A., Garcia, R. R., and Roble, R.: Effect of El Niño-Southern Oscillation on the dynamical, thermal, and chemical structure of the middle atmosphere, *J. Geophys. Res.*, 109, D17108, doi:10.1029/2003JD004434, 2004.
- Sato, M., Hansen, J. E., McCormick, M. P., and Pollack, J. B.: Stratospheric aerosol optical depths, 1850–1990, *J. Geophys. Res.*, 98, 22987–22994, 1993.
- Scaife, A. A., Kucharski, F., Folland, C. K., Kinter, J., Brönnimann, S., Fereday, D., Fischer, A. M., Grainger, S., Jin, E. K., Kang, I. S., Knight, J. R., Kusunoki, S., Lau, N. C., Nath, M. J., Nakaegawa, T., Pegion, P., Schubert, S., Sporyshev, P., Syktus, J., Yoon, J. H., Zeng, N., and Zhou, T.: The CLIVAR C20CR project: selected 20th century climate events, *Clim. Dynam.*, 33, 603–614, 2008.
- Schraner, M., Rozanov, E., Schnadt Poberaj, C., Kenzelmann, P., Fischer, A. M., Zubov, V., Luo, B. P., Hoyle, C. R., Egorova, T., Fueglistaler, S., Brönnimann, S., Schmutz, W., and Peter, T.: Technical Note: Chemistry-climate model SOCOL: version 2.0 with improved transport and chemistry/microphysics schemes, *Atmos. Chem. Phys.*, 8, 5957–5974, doi:10.5194/acp-8-5957-2008, 2008.
- SPARC CCMVal: SPARC Report on the Evaluation of Chemistry-Climate Models, in: SPARC Report No. 5, edited by: Eyring, V., Shepherd, T. G., and Waugh, D. W., WCRP-132, WMO/TD-No. 1526, available online at: http://library.wmo.int/pmb_ged/wmo-td_1526.pdf, 2010.
- Staehelin, J., Renaud, A., Bader, J., McPeters, R., Viatte, P., Hoegger, B., Buignion, V., Giroud, M., and Schill, H.: Total ozone series at Arosa (Switzerland): homogenisation and data comparison, *J. Geophys. Res.*, 103, 5827–5841, 1998.

A global historical ozone data set

S. Brönnimann et al.

Title Page

Abstract

Introduction

Conclusions

References

Tables

Figures

◀

▶

◀

▶

Back

Close

Full Screen / Esc

Printer-friendly Version

Interactive Discussion



- Stolarski, R. S. and Frith, S. M.: Search for evidence of trend slow-down in the long-term TOMS/SBUV total ozone data record: the importance of instrument drift uncertainty, *Atmos. Chem. Phys.*, 6, 4057–4065, doi:10.5194/acp-6-4057-2006, 2006.
- Stolarski, R. S., Labow, G. J., and McPeters, R. D.: Springtime Antarctic total ozone measurements in the early 1970s from the BUV instrument on Nimbus 4, *Geophys. Res. Lett.*, 24, 591–594, 1997.
- Svendby, T. M.: Reanalysis of total ozone measurements at Dombås and Oslo, Norway, from 1940 to 1949, *J. Geophys. Res.*, 108, 4750, doi:10.1029/2003JD003963, 2003.
- Taylor, K. E., Stouffer, R. J., and Meehl, G. A.: An overview of CMIP5 and the experiment design, *B. Am. Meteorol. Soc.*, 93, 485–498, doi:10.1175/BAMS-D-11-00094.1, 2012.
- Tie, X. X. and Brasseur, G.: The response of stratospheric ozone to volcanic-eruptions – sensitivity to atmospheric chlorine loading, *Geophys. Res. Lett.*, 22, 3035–3038, 1995.
- Uppala, S. M., Kållberg, P. W., Simmons, A. J., Andrae, U., Bechtold, V. Da Costa, Fiorino, M., Gibson, J. K., Haseler, J., Hernandez, A., Kelly, G. A., Li, X., Onogi, K., Saarinen, S., Sokka, N., Allan, R. P., Andersson, E., Arpe, K., Balmaseda, M. A., Beljaars, A. C. M., Berg, L. Van De, Bidlot, J., Bormann, N., Caires, S., Chevallier, F., Dethof, A., Dragosavac, M., Fisher, M., Fuentes, M., Hagemann, S., Hólm, E., Hoskins, B. J., Isaksen, L., Janssen, P. A. E. M., Jenne, R., McNally, A. P., Mahfouf, J.-F., Morcrette, J.-J., Rayner, N. A., Saunders, R. W., Simon, P., Sterl, A., Trenberth, K. E., Untch, A., Vasiljevic, D., Viterbo, P., and Woollen, J.: The ERA-40 re-analysis, *Q. J. Roy. Meteorol. Soc.*, 131, 2961–3012, 2005.
- Vogler, C., Brönnimann, S., and Hansen, G.: Re-evaluation of the 1950–1962 total ozone record from Longyearbyen, Svalbard, *Atmos. Chem. Phys.*, 6, 4763–4773, doi:10.5194/acp-6-4763-2006, 2006.
- Vogler, C., Brönnimann, S., Staehelin, J., and Griffin, R. E. M.: The Dobson total ozone series of Oxford: re-evaluation and applications, *J. Geophys. Res.*, 112, D20116, doi:10.1029/2007JD008894, 2007.
- Whitaker, J. S. and Hamill, T. M.: Ensemble data assimilation without perturbed observations, *Mon. Weather Rev.*, 130, 1913–1924, 2002.
- Williamson, D. L. and Rasch, P. J.: Two-dimensional semilagrangian transport with shape-preserving interpolation, *Mon. Weather Rev.*, 117, 102–129, 1989.
- WMO, World Meteorological Organization: Report of the WMO Meeting of Experts on Assessments of Performance Characteristics of Various Ozone Measuring Systems, Global Ozone Research and Monitoring Project, Report 9, WMO, Geneva, 1980.

WMO: Review of the Dobson Spectrophotometer and its Accuracy, Global Ozone Research and Monitoring Project, Report 13, WMO, Geneva, 1983.

Zubov, V. A., Rozanov, E. V., and Schlesinger, M. E.: Hybrid scheme for three-dimensional advective transport, Mon. Weather Rev., 127, 1335–1346, 1999.

ACPD

13, 7767–7809, 2013

A global historical ozone data set

S. Brönnimann et al.

Title Page

Abstract

Introduction

Conclusions

References

Tables

Figures

⏪

⏩

◀

▶

Back

Close

Full Screen / Esc

Printer-friendly Version

Interactive Discussion



A global historical ozone data set

S. Brönnimann et al.

Table 1. Selection of Strong El Niño and La Niña winters (January–March) following Brönnimann et al. (2007).

El Niño		La Niña	
pre-1979	post-1979	pre-1979	post-1979
1940	1987	1934	1985
1941	1998	1943	1989
1952	2003	1950	2000
1958		1956	
1966		1968	
1973		1971	
1977		1974	
		1976	

[Title Page](#)
[Abstract](#)
[Introduction](#)
[Conclusions](#)
[References](#)
[Tables](#)
[Figures](#)
[I◀](#)
[▶I](#)
[◀](#)
[▶](#)
[Back](#)
[Close](#)
[Full Screen / Esc](#)
[Printer-friendly Version](#)
[Interactive Discussion](#)


A global historical ozone data set

S. Brönnimann et al.

Title Page

Abstract

Introduction

Conclusions

References

Tables

Figures

◀

▶

◀

▶

Back

Close

Full Screen / Esc

Printer-friendly Version

Interactive Discussion



Table 2. Definition of periods of solar maxima and minima.

pre-1979	Maxima		pre-1979	Minima	
		post-1979			post-1979
Dec 1936 to Nov 1938	May 1979 to Apr 1981	Apr 1943 to Mar 1945	Apr 1985 to Mar 1987	Apr 1943 to Mar 1945	Apr 1985 to Mar 1987
Apr 1947 to Mar 1949	Dez 1988 to Nov 1990	Feb 1953 to Jan 1955	Aug 1995 to Jul 1997	Feb 1953 to Jan 1955	Aug 1995 to Jul 1997
Apr 1957 to Mar 1959	Feb 2000 to Jan 2002	Dec 1963 to Nov 1965	Sep 2007 to Aug 2009*	Dec 1963 to Nov 1965	Sep 2007 to Aug 2009*
Aug 1968 to Jul 1970		Feb 1975 to Jan 1977		Feb 1975 to Jan 1977	

* We used Jan–Dec 2007 for the last minimum as BDBP ends in 2007.

A global historical ozone data set

S. Brönnimann et al.

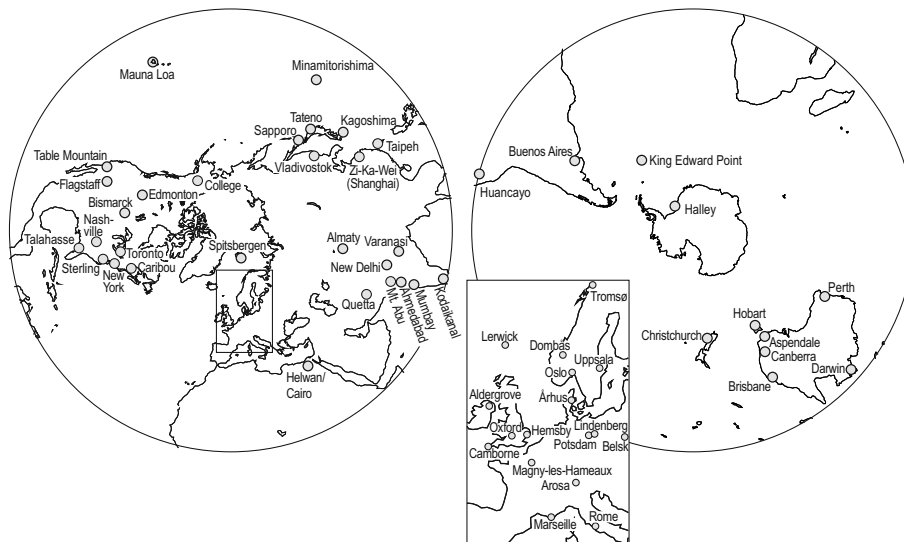


Fig. 1. Map showing the locations of the ground-based total column ozone stations used in this study.

Title Page

Abstract

Introduction

Conclusions

References

Tables

Figures

◀

▶

◀

▶

Back

Close

Full Screen / Esc

Printer-friendly Version

Interactive Discussion



**A global historical
ozone data set**

S. Brönnimann et al.

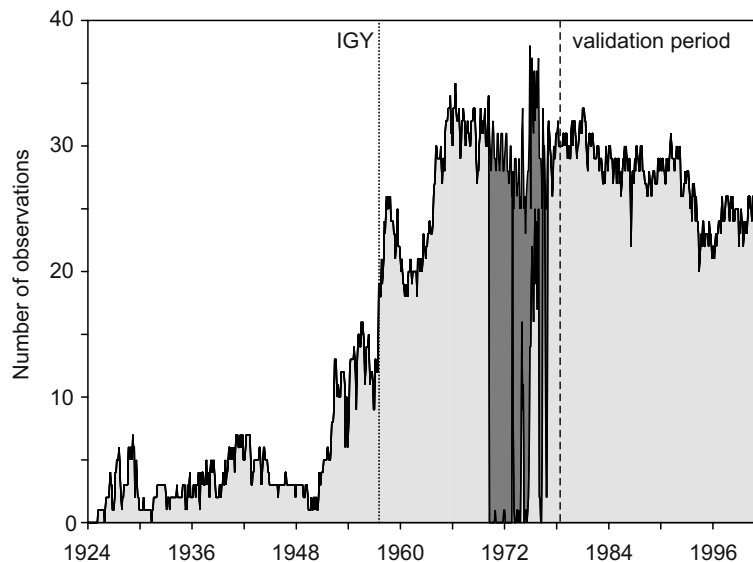


Fig. 2. Number of monthly mean values assimilated in the assimilation period (1925–1978) and validation period (1979–1999). Ground-based and BUV data are shown in light and dark grey shading, respectively.

[Title Page](#)[Abstract](#)[Introduction](#)[Conclusions](#)[References](#)[Tables](#)[Figures](#)[◀](#)[▶](#)[◀](#)[▶](#)[Back](#)[Close](#)[Full Screen / Esc](#)[Printer-friendly Version](#)[Interactive Discussion](#)

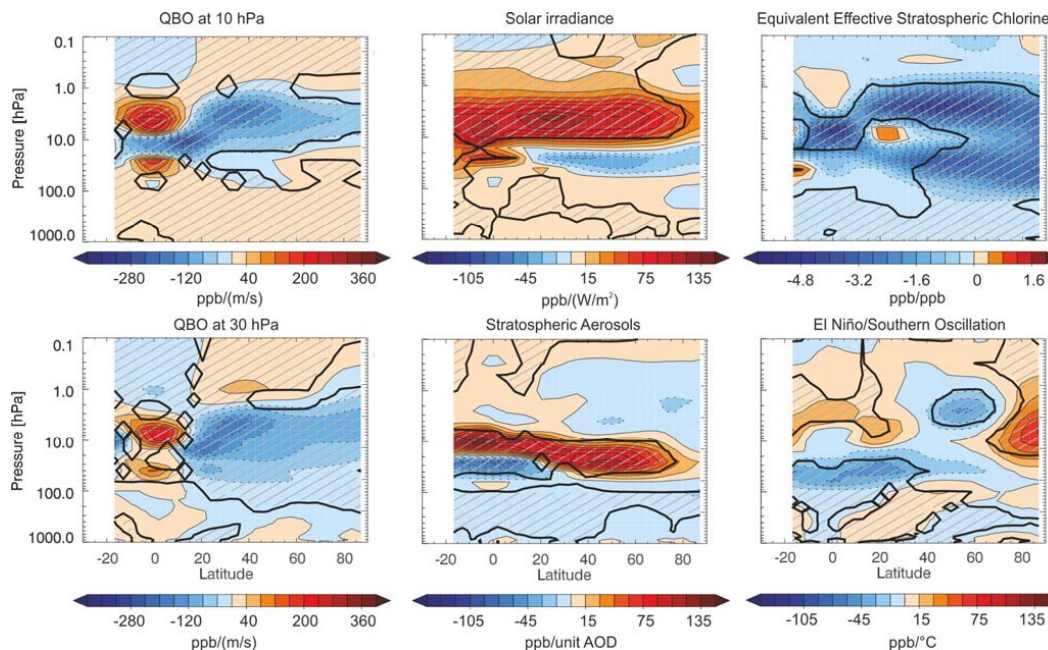


Fig. 3. Coefficients of a multiple regression model with zonal mean ozone mixing ratios of the ensemble mean as predictand and various predictor variables. Shaded areas, together with black contour line, mark statistically significant areas (p -value < 0.05). For comparability reasons the regression-coefficients are displayed as ppbv change with respect to one standard deviation of the predictor. Due to the long-term trend in EESC, however, this coefficient is plotted with respect to 100 pptv.

Title Page

Abstract

Introduction

Conclusions

References

Tables

Figures

◀

▶

◀

▶

Back

Close

Full Screen / Esc

Printer-friendly Version

Interactive Discussion



A global historical ozone data set

S. Brönnimann et al.

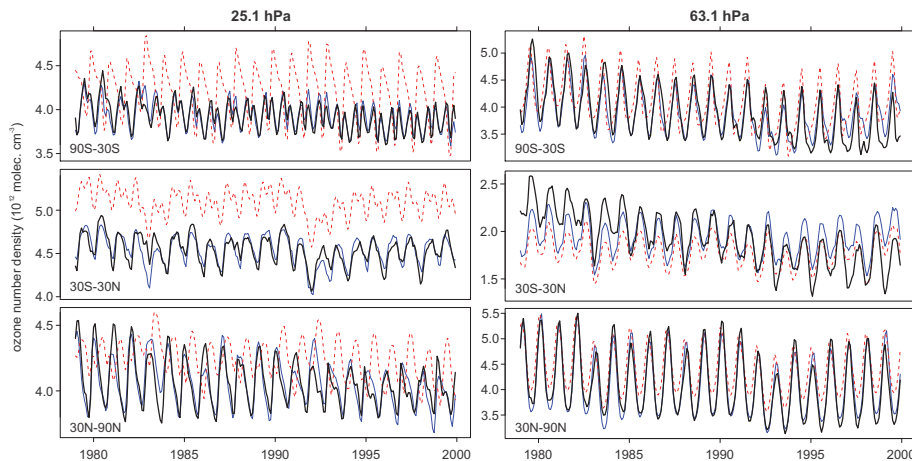


Fig. 4. Comparison of ozone at two levels and in three latitude regions from the original SOCOL simulations (red dotted), debiased SOCOL simulations (blue) and BDBP (thick black).

Title Page

Abstract

Introduction

Conclusions

References

Tables

Figures

◀

▶

◀

▶

Back

Close

Full Screen / Esc

Printer-friendly Version

Interactive Discussion



A global historical ozone data set

S. Brönnimann et al.

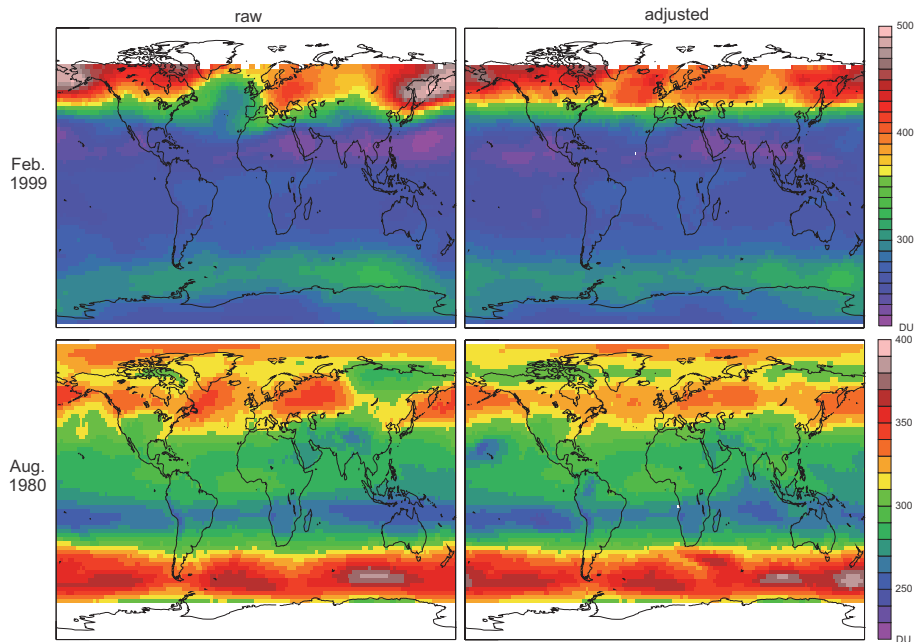


Fig. 5. Comparison of raw and zonally adjusted TOMS total column ozone data for February 1999 and August 1980.

[Title Page](#)[Abstract](#)[Introduction](#)[Conclusions](#)[References](#)[Tables](#)[Figures](#)[◀](#)[▶](#)[◀](#)[▶](#)[Back](#)[Close](#)[Full Screen / Esc](#)[Printer-friendly Version](#)[Interactive Discussion](#)

A global historical ozone data set

S. Brönnimann et al.

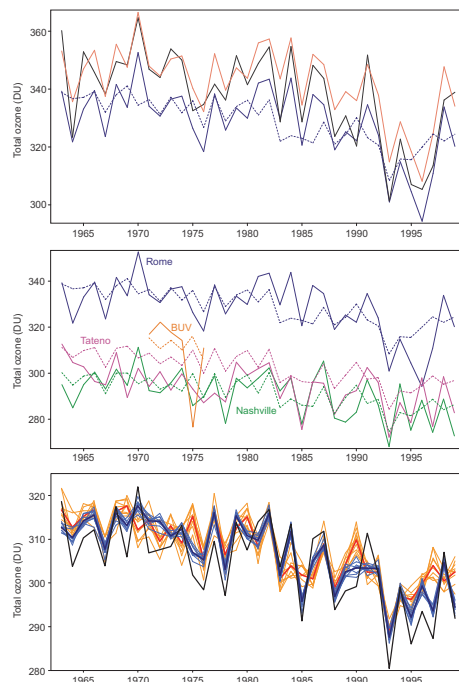


Fig. 6. Example of the pre-processing steps of monthly mean total column ozone observation series performed in this paper. Top: comparison of raw series (black), zonally adjusted series (orange), debiased series (blue solid), and ensemble mean background (debiased SOCOL, blue dashed) for the case of Rome. Middle: debiased observations (solid) and ensemble mean background (debiased SOCOL, dashed) for Rome, Tateno, Nashville, and BUJ data at 35–40° N. Bottom: comparison of debiased observations (black), background (ensemble mean and members, red and orange) and the final HISTOZ.1.0 product (ensemble mean and members, dark and light blue) for the average of the three stations Rome, Tateno, Nashville.

[Title Page](#)
[Abstract](#)
[Introduction](#)
[Conclusions](#)
[References](#)
[Tables](#)
[Figures](#)
[◀](#)
[▶](#)
[◀](#)
[▶](#)
[Back](#)
[Close](#)
[Full Screen / Esc](#)
[Printer-friendly Version](#)
[Interactive Discussion](#)

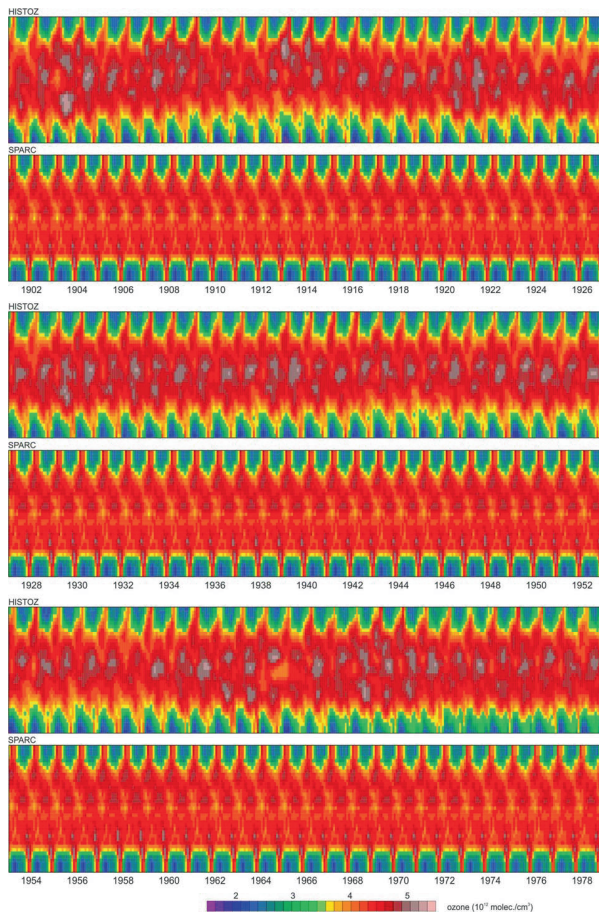



Fig. 7. Latitude-time cross-section of HISTOZ.1.0, the SPARC data set, and BDBP (after 1979 only) at 25.1 hPa from 1901 to 2004.

A global historical ozone data set

S. Brönnimann et al.

Title Page

Abstract Introduction

Conclusions References

Tables Figures

◀ ▶

◀ ▶

Back Close

Full Screen / Esc

Printer-friendly Version

Interactive Discussion



A global historical ozone data set

S. Brönnimann et al.

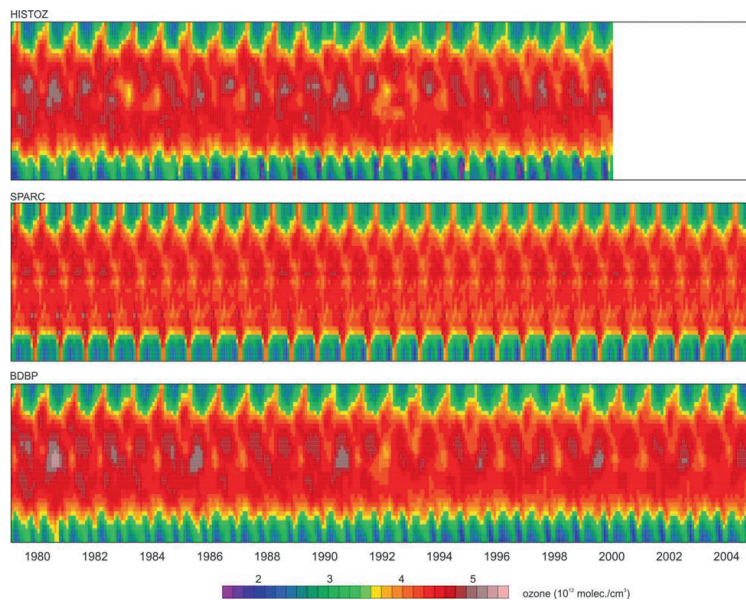


Fig. 7. Continued.

Title Page

Abstract

Introduction

Conclusions

References

Tables

Figures

◀

▶

◀

▶

Back

Close

Full Screen / Esc

Printer-friendly Version

Interactive Discussion



A global historical ozone data set

S. Brönnimann et al.

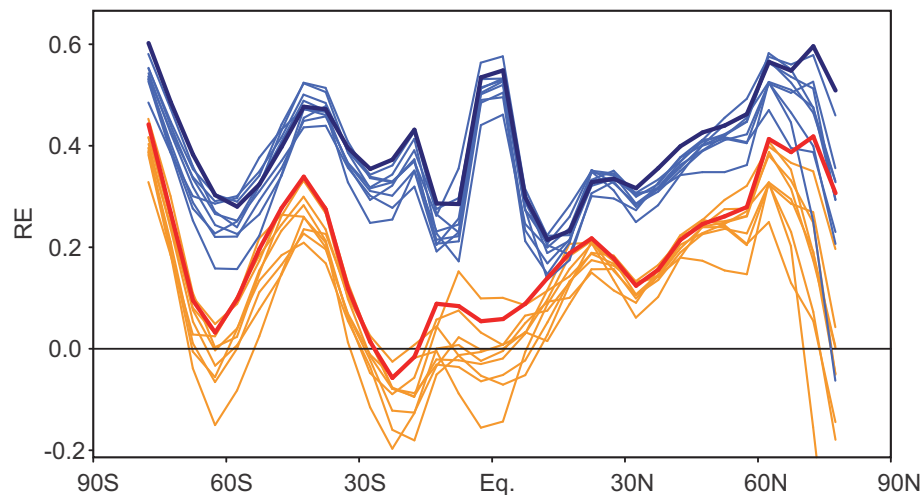


Fig. 8. RE values for total column ozone (monthly means) derived from comparing HISTOZ.1.0 with TOMS. Thick lines are for the ensemble mean, thin line for the members. Blue refers to h_0 : climatology of x_b , orange refers to h_0 : x_b .

Title Page

Abstract

Introduction

Conclusions

References

Tables

Figures

◀

▶

◀

▶

Back

Close

Full Screen / Esc

Printer-friendly Version

Interactive Discussion



A global historical ozone data set

S. Brönnimann et al.

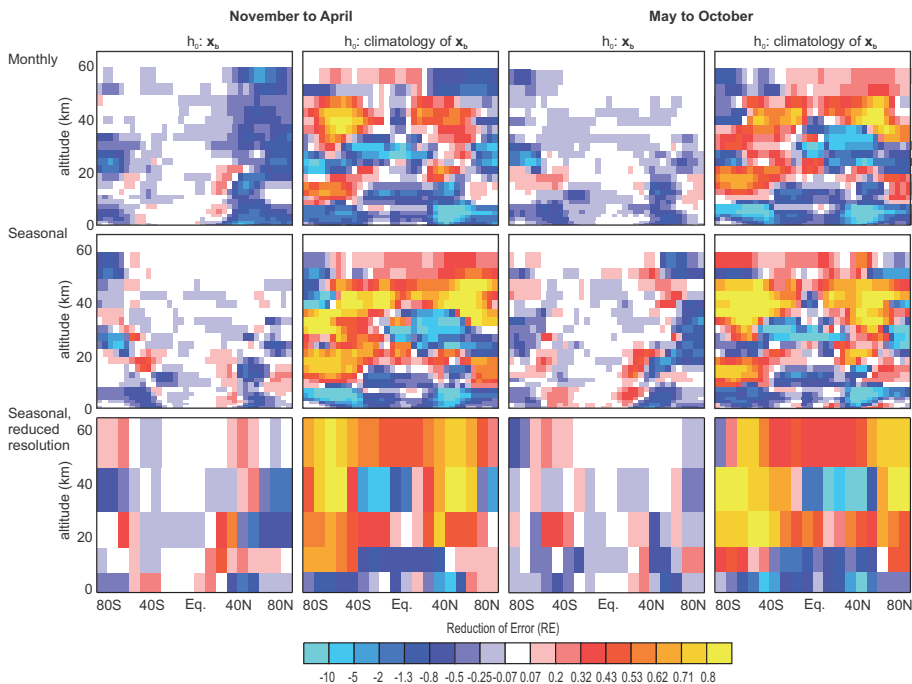


Fig. 9. RE values for the vertical ozone distribution derived from comparing HISTOZ.1.0 with BDBP (only for the ensemble mean) for boreal winter and summer periods.

Title Page

Abstract Introduction

Conclusions References

Tables Figures

◀ ▶

◀ ▶

Back Close

Full Screen / Esc

Printer-friendly Version

Interactive Discussion



A global historical ozone data set

S. Brönnimann et al.

Title Page

Abstract

Introduction

Conclusions

References

Tables

Figures

◀

▶

◀

▶

Back

Close

Full Screen / Esc

Printer-friendly Version

Interactive Discussion

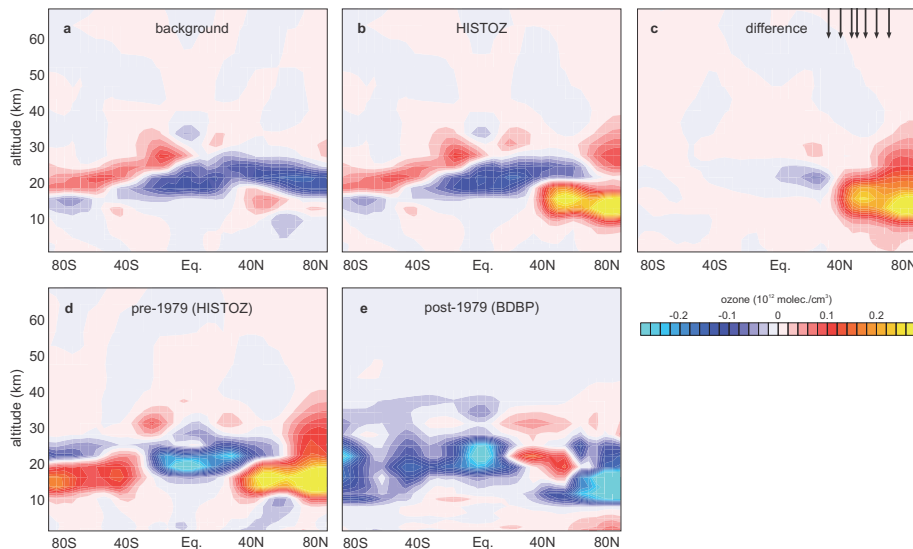


Fig. 10. Ozone differences for annual means of 1940–1942 minus those of the years 1939, 1943, and 1944 for (a) the background, (b) HISTOZ.1.0) and (c) the difference HISTOZ.1.0 minus background. Arrows indicate locations where observations were assimilated. The lower row show differences in January–March averages for El Niño minus La Niña winters (see Table 3) for the pre-1979 period (d, based on HISTOZ.1.0) and the post-1979 period (e, BDBP). Percentage deviations are shown in Fig. S4.

A global historical ozone data set

S. Brönnimann et al.

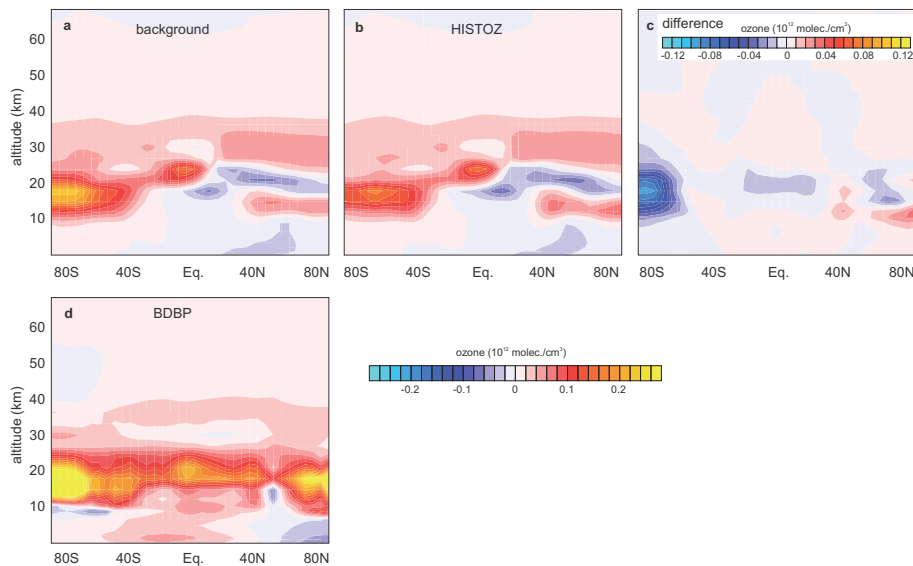


Fig. 11. Ozone differences for solar maximum minus solar minimum (see Table 4) prior to 1979 in **(a)** the background, **(b)** HISTOZ.1.0 and **(c)** the difference HISTOZ.1.0 minus background. Panel **(d)** shows corresponding differences in the post-1979 period (BDBP). Percentage deviations are shown in Fig. S4.

Title Page

Abstract

Introduction

Conclusions

References

Tables

Figures

◀

▶

◀

▶

Back

Close

Full Screen / Esc

Printer-friendly Version

Interactive Discussion

